Parametric Study of HEMP-Thruster, Downscaling to µN Thrust Levels

IEPC-2013-269

Presented at the 33rd International Electric Propulsion Conference,
The George Washington University, Washington, D.C., USA
October 6–10, 2013

Andreas Keller,*
Astrium GmbH - Satellites, Friedrichshafen, Germany
Justus-Liebig-University Gießen, I. Physikalisches Institut, Germany

Peter Köhler,
Justus-Liebig-University Gießen, I. Physikalisches Institut, Germany

Franz Georg Hey,
Astrium GmbH - Satellites, Friedrichshafen, Germany
Technische Universität Dresden, Germany

Marcel Berger,
Astrium GmbH - Space Transportation, Bremen, Germany

Claus Braxmaier,
University of Bremen, ZARM Center of Applied Space Technology and Microgravity
DLR German Aerospace Center, Institute of Space Systems, Bremen

Davar Feili,
University of Southampton, Faculty of Engineering and the Environment, United Kingdom

Dennis Weise, Ulrich Johann
Astrium GmbH - Satellites, Friedrichshafen, Germany

Abstract: Many on-going ESA's science and Earth Observation missions are based on fine attitude control and formation flying. All these missions apply strong requirements on propulsion system which should provide low thrust and high precision thrust vectors in up to 16 directions. Also as the most of these missions have a platform with small solar cell arrays, the power consumption of the propulsion system should be very low.

The idea of using a small HEMP thruster for such missions is very attractive due its relatively low subsystem complexity and low system mass. So the ability of down-scaling a HEMP-T to the µN range is investigated experimentally. A measurement campaign studying systematically the influence of the geometrical dimensions of main thruster parts on operation, beam profile and ion acceleration is presented. Additionally the anode material was varied which shows an impact to ion acceleration distribution.

The minimum achieved thrust was 50 µN and 70 s by 350 V anode voltage.

*Andreas.Keller@exp1.physik.uni-giessen.de

Nomenclature

HEMPT	High Efficiency Multistage Plasma Thruster
FD	Faraday Array
RPA	Retarding Potential Analyser
OS	Operation space
DiMagnet	Inner diameter of magnet hole
DoMagnet	Outer diameter of magnet ring
DistMagnet	Distance between two magnets
NumberMagnet	Quantity of magnets
DiDchamber	Inner diameter of discharge chamber

I. Introduction

UPCOMING satellite missions such as eLISA, LISA Pathfinder, GRACE, GAIA, DARWIN, and EUCLID require increasing precision pointing and positioning combined with long life time. The HEMP (High Efficiency Multistage Plasma) thruster technology[4] has promising properties with respect to system simplicity and erosion free characteristics. Typically, HEMP thruster developments aim at thrust ranges in the mN range[2] which is adequate for position and orbit control of mid-size satellites while there is still a deficit in the µN range.

We investigate experimentally the ability of down-scaling the HEMP thruster concept into the µN thrust range. This means building up and characterising of thruster hardware as well as verification of simple models. A comprehensive particle-in-cell simulation is performed in coorporation at DLR in Bremen.[1] After investigating the influence of electric and magnetic susceptibility of housing material on beam divergence which was presented on last IEPC,[3] a measurement campaign was performed covering a systematic variation of geometry parameters such as discharge chamber diameter (2 to 5 mm), strength of magnetic field (via the outer diameter of SmCo magnet from 10 to 40 mm), cusp length (1 to 10 mm), and number of cusps (up to three).

The different thruster configurations were characterised in a turbo and cryo pumped vacuum chamber by their operation space (lowest possible mass flow with a given anode voltage) as well as the beam profile. Retarding Potential Analyser and Faraday Array measurements can be calculated to a divergence and acceleration efficiency which leads to precise thrust and specific impulse assumptions. These values are compared within and between the measurement series, respectively. Thrusts down to 130 µN and 320 s, 100 µN and 250 s as well as 50 µN and 70 s are observed.

Additionally to the geometry parameters the anode material was varied. By changing the material from aluminum to copper or brass the difference between maximum acceleration voltage of ions and anode voltage can be reduced from 50 to 5 V which increases acceleration efficiency. The scope, test setup and the analysis of the measurement series is presented.

II. Thruster design

The HEMP thruster is based on the principle of electron bombardment ionisation and ion acceleration in the same electric field, generated by the anode (see Fig. 1). The ring shaped periodically poled permanent magnets create several cusp areas with radial magnetic field, where the electrons oscillate on Larmor radii to increase the interaction length and to reduce wall erosion.[4]

Designing a HEMP-T for low thrusts is a difficult task due to the complex nature of the HEMP-T physics. In this work the experimental approach is chosen with building up prototypes which are tested. The most influential geometry parameters of thruster are identified and systematically varied. The resulting test thruster are characterised for operation stability, beam profile and ion acceleration voltage (parameter mapping). Correlations of parameters are not part of survey and should be avoided.

The considered geometrical parameters correspond to functional parameters as:

- Neutral gas pressure in discharge chamber via DiDchamber: The magnet dimensions are fixed (K1-K3) as well as magnet hole minimised (K8, K5, K3, K23)

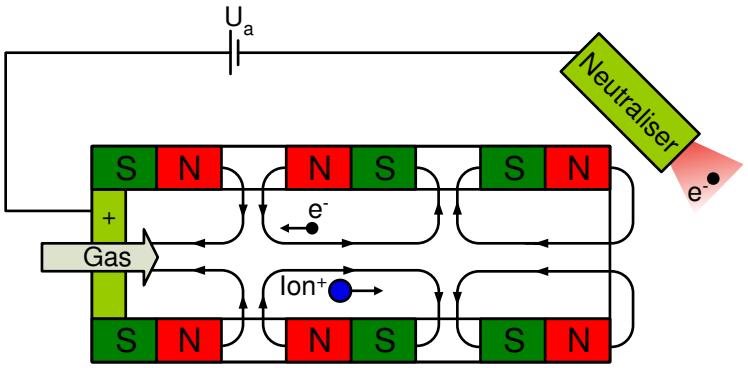

Figure 1. HEMP-T principle

- Variation of magnetic field strength via DoMagnet
- Number of cusps via NumberMagnet
- Size of cusps via DistMagnet

For the list of characterised configurations, see Table 1. All thrusters use magnets rings of SmCo, a cylindrical discharge chamber of alumina and Xenon as propellant. The anode is made of aluminium except for K26 (see section III.C).

Cfg	DiMagnet	DoMagnet	NumberMagnet	DiDchamber	DistMagnet
K1	6.4			2	
K2	6.4			3	
K3	6.4			5	
K4		40			
K5	4.4	30	3	3	2.5
K6		20			
K7		10			
K8	3.4			2	
K5	4.4			3	
K3	6.4			5	
K23	10.6			8	
K11					1
K5					2.5
K13					5
K14					10
K15			2		
K5			3		
K17			4		

Table 1. List of all thruster configurations. K5 is baseline device and exclusively varied values are given in the other lines. The units are mm.

III. Characterisation

The work was concentrated in two main directions; in the first direction a minimum thrust should be achieved, which would make the thruster able for fine position and attitude controlling manoeuvres. In the second stage a precise correlation between the thrust and the measureable operating parameters of the thruster should be established. This would give a measure of the thrust by measuring the thruster parameters like voltage, current and gas flow. In order to reduce the thrust of HEMP thruster needs to be measured:

- lowest operational mass flow with a fixed anode voltage which can be derived to minimum thrust and corresponding specific impulse
- divergence efficiency as beam geometry parameter
- acceleration efficiency

Within a test series these values are compared with the different configurations so that the influence of the parameter on the measured values are studied. The thrusters are designed as universal as possible in order to minimise correlation between different design parameters. As example the same housing size was used for all configurations (see Fig. 2) because the grounded housing acts as electrode and delivers free electrons. Additionally the influence of anode material on acceleration efficiency was measured.

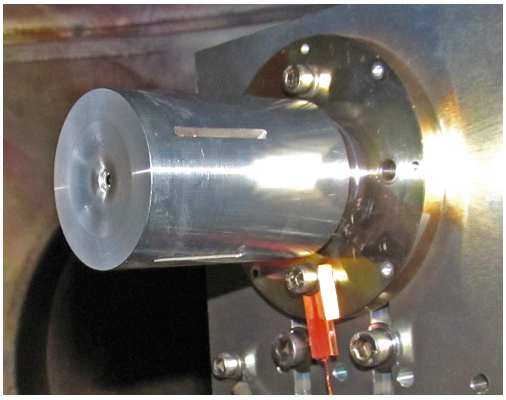

Figure 2. µHEMP thruster

For a precise determination of the thrust using the anode current and voltage a characterization of the electric fields inside and outside the thruster is necessary, as they define the velocity of the ions coming out of the thruster and sowith the Isp. It can be done by measuring the ion energy distribution and beam current in different angels. The characterisation was performed at R2D2 – test facility in Giessen with a faraday array and a RPA (see Fig. 3). The 32-Cup Faraday Array with a resolution of 1.4e−5µA/mm^2 can be rotated 330 ° around the thruster in order to quantify the ion current density versus the angular position. On these positions the acceleration voltage of ions can be determined using a Retarding Potential Analyser with three grids.

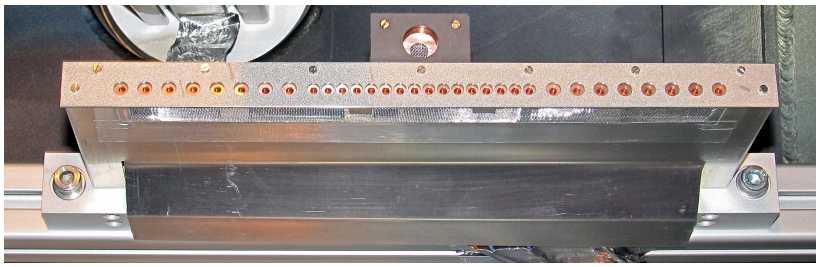

Figure 3. Image of Faraday Array and Retarding Potential Analyser.

A. Calculation of thrust

The Thrust F, momentum p, propellant mass flow $\dot{m}_p$ and velocity of ions v_{ion}

$$F = \dot{p} = \dot{m}_p v_{\text{ion}} \tag{1}$$

calculates with conservation of energy

$$eU = \frac{1}{2} m_{\text{ion}} v_{\text{ion}}^2 \tag{2}$$

to

$$F_0 = I_b \times \sqrt{2U m_{\text{ion}}/e}, \tag{3}$$

where $I_b = e\dot{m}_p/m_{\text{ion}}$ denotes the electrical beam current and U the difference of electric potential. Here the assumption of only single ionized particles with elementary charge e is made.

It is assumed that all ions leave the thruster directly in thruster axis. However, most ion vectors are tilted to thruster axis (denoted as φ) which reduces the effective thrust by the factor of $\cos\varphi$. Angular independent equation 3 can be seen as sum of forces F_φ applied on ions travelling into direction φ:

$$F_0 = \sum_\varphi F_\varphi \tag{4}$$

In order to apply the geometrical factor, F_φ is multiplied with $\cos\varphi$

$$F_1 = \sum_\varphi F_\varphi \times \cos\varphi = F_0 \times \frac{\sum_\varphi F_\varphi \times \cos\varphi}{F_0} = F_0 \times \eta_{\text{div}}, \tag{5}$$

which defines divergence efficiency

$$\eta_{\text{div}} = \frac{\sum_\varphi F_\varphi \times \cos\varphi}{\sum_\varphi F_\varphi}. \tag{6}$$

The force F_φ is determined by Faraday Cups which measures current density in dependance of φ. Raw current captured in Faraday cup $I_{\text{raw},\varphi}$ was calculated with dark current $I_{\text{dark},\varphi}$ and the acceptance area of cups A_{cup} to current density ρ_φ

$$\rho_\varphi = \frac{I_{\text{raw},\varphi} - I_{\text{dark},\varphi}}{A_{\text{cup}}}. \tag{7}$$

The total electrical current in a half spherical segment $I_{\text{total},\varphi}$ (the current density is measured for negative and positive angles) with radius of sphere R calculates from current density multiplied by half segment area

$$A_{\text{seg}} = 2\pi R^2(\cos(\varphi - \Delta\varphi/2) - \cos(\varphi + \Delta\varphi/2))/2 = 2\pi R^2(2\,|\sin\varphi|\sin\Delta\varphi/2)/2 \tag{8}$$

which scales with $|\sin\varphi|$ in the angle. So larger planar angles feature a stronger influence in divergence efficiency than small angles. The total current calculates to

$$I_{\text{total},\varphi} = \rho_\varphi \times 2\pi R^2(\cos(\varphi - \Delta\varphi/2) - \cos(\varphi + \Delta\varphi/2))/2. \tag{9}$$

Here the spacing between two measurement points $\Delta\varphi$ is equidistant. The force on all ions travelling in direction φ is directly proportional to the total current $I_{\text{total},\varphi}$ by comparing $\sum_\varphi I_{\text{total},\varphi} = I_b$ with equation 4:

$$F_\varphi = I_{\text{total},\varphi} \times \sqrt{2U m_{\text{ion}}/e}. \tag{10}$$

This leads to

$$\eta_{\text{div}} = \frac{\sum_\varphi I_{\text{total},\varphi} \times \cos\varphi}{\sum_\varphi I_{\text{total},\varphi}}. \tag{11}$$

Equation 10 assumes that all ions passed the same potential drop U, but the RPA measurements shows that this is not valid for most ions. In Fig. 4 RPA measurements for different angles are given. Only at the maximum emission angle at $-55°$ a full potential passage of anode voltage U_a can be assumed but for larger angles the main peak of derivative shifts to lower voltages.

These low voltage ions may be produced downstream where the plasma potential is lower than anode potential or may occur due to inelastic collisions of ions with other ions which can also explain the larger angles.

This behaviour can be expressed by splitting the maximum RPA current $I_{\mathrm{total},\varphi} \propto \sum_i \Delta I_i$ in small current steps and multiplying them with the square root of corresponding retarding voltage U_i:

$$F_\varphi = \sum_i \Delta I_i \sqrt{U_i} \times \sqrt{2 m_{\mathrm{ion}}/e} = I_{\mathrm{total},\varphi} \sqrt{U_a} \times \frac{\sum_i \Delta I_i \sqrt{U_i}}{I_{\mathrm{total},\varphi} \sqrt{U_a}} \times \sqrt{2 m_{\mathrm{ion}}/e}. \tag{12}$$

which defines an angular dependant acceleration efficiency

$$\eta_{\mathrm{acc},\varphi} = \frac{\sum_i \Delta I_i \sqrt{U_i}}{I_{\mathrm{total},\varphi} \sqrt{U_a}}. \tag{13}$$

Now thrust calculates to

$$F_1 = \sum_\varphi I_{\mathrm{total},\varphi} \sqrt{2 U_a m_{\mathrm{ion}}/e} \times \eta_{\mathrm{acc},\varphi}. \tag{14}$$

From this a total acceleration efficiency can be calculated by carrying out the sum over all angles:

$$\eta_{\mathrm{acc}} = \frac{\sum_\varphi I_{\mathrm{total},\varphi} \eta_{\mathrm{acc},\varphi}}{\sum_\varphi I_{\mathrm{total},\varphi}}, \tag{15}$$

so thrust writes as

$$F_1 = \eta_{\mathrm{acc}}\, \eta_{\mathrm{div}}\, F_0. \tag{16}$$

Due to measurement process, ΔI_i is calculated as derivative of current $I(U_i)$ which is supposed to be negative because more and more ions are repelled with increasing retarding voltage. Noise and ion optic effects at the retarding grid may result to positive derivatives which needs to be removed at the calculation. Therefore a function is fitted to the measured values which has a strictly negative derivative. Here a sigmoidal Boltzmann function is used, which fits the measured data very well:

$$f(x) = a + \frac{b}{1 + e^{(x-c)/d}}. \tag{17}$$

The derivative calculates to

$$\frac{df}{dx} = \frac{-b(e^{(x-c)/d})}{d(1 + e^{(x-c)/d})^2} \tag{18}$$

and can be forced to be negative if the fit parameter $b > 0$ is limited to positive values ($d > 0$ needs also to be positive since the parameters means the width of drop-off zone). Several Boltzmann terms are summed in order to reproduce all steps. These fitting curves are shown in Fig. 4 as solid lines.

RPA measurements are performed on a few angles. For the intermediate angles and in the outer range where the current is too low for a precise measurement, the acceleration efficiencies needs to be inter- and extrapolated. Therefore a fitting curve is used which can be of Gaussian type:

$$f(x) = y_0 + \frac{A}{w\sqrt{\pi/2}} \exp -2(x - x_c)^2/w^2 \tag{19}$$

In Fig. 5 an example is shown. The solid blue curve is a Gaussian fit to the measurement points (blue circles). As comparison the beam profile as relative ion current is shown as red solid curve. The maximum of ion emission and maximum of acceleration efficiency is in the same angular range which leads to a high efficiency. The possible error of the extrapolated area has limited influence in calculated thrust because the beam current is rather low (this presumably also counteracts the larger sphere segment area in the higher angles).

Manual tuning of startpoints and number of terms of the RPA fits and removing of double measurements which are inconsistent with each other because they are recorded on different days are effecting the efficency value only marginally. Two of the 275 measurements are changed by 5% but most are changed by 1% and less which effects the thrust by less than 3 µN and thus can be neglected.

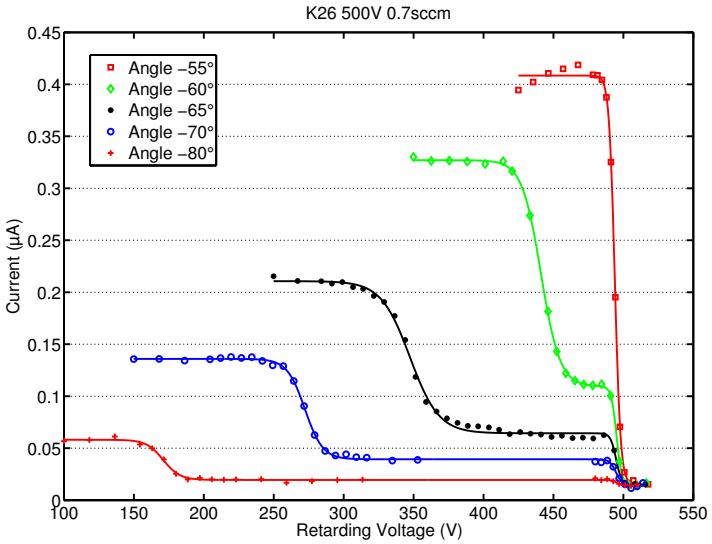

Figure 4. RPA current for K26 (equal to K5 except with brass anode) with anode voltage of $500\,V$, mass flow of 0.7 sccm measured at different angles. The fitting curve is given in the corresponding colour as solid line.

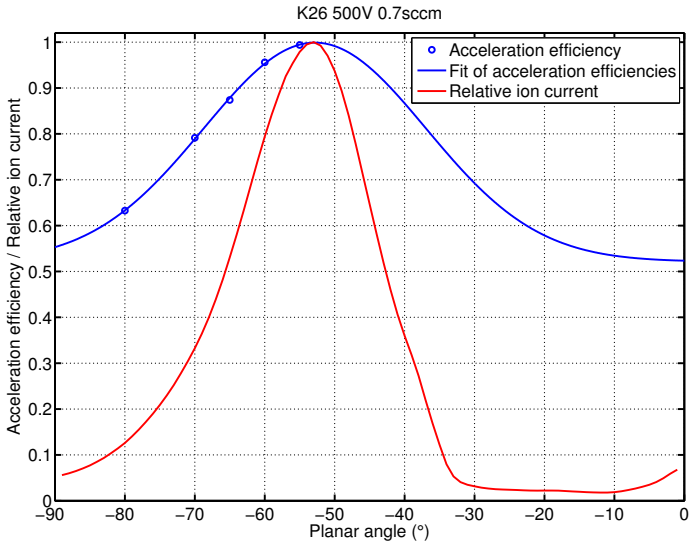

Figure 5. Acceleration efficiencies of K26 plotted versus the planar angle. The fitting curve is shown as blue solid curve. As comparison the beam profile as relative ion current is shown as red solid curve.

Limiting the maximum of gaussion curve in the fitting process to 1 by adjusting the boundaries of center angle x_c results in decreasing of some values which is necessary because efficiencies larger unity are physically impossible. This has an impact of maximal 9%.

The shown procedure is used in the test campaign to calculate thrust and Isp from beam profile and RPA data. Nevertheless must be considered that the thrusts are calculated and do not supersede direct thrust measurements on a balance.

B. Test campaign

The following results of test campaign are exemplary and all test series are summarized in Table 1.

1. Operation space

In Fig. 6 the minimal mass flows are plotted versus the anode voltage for different inner discharge chamber diameters which corresponds to the neutral gas density. The curves for K2 and K3 are shown while the thruster with the smallest discharge chamber, K1, could not be operated because the spacing between discharge chamber wall and magnet hole was too large. Thus electron loss rate at the walls is too high so that no stable plasma discharge can be established.

The thruster with the larger discharge chamber requires higher mass flows to operate and accepts as well as requires higher anode voltages. Higher mass flows are needed due to the lower resistance of a large channel in order to obtain the same neutral gas density. The mass flows of K2 are on average $89 \pm 3\,\%$ of the larger one (in the voltage overlap). The pressure decrease may be counteracted by larger possible larmor radii so that also the slower electrons do not collide with the walls. The higher voltages can also be accounted on larger radii because it is directly proportional to electron velocity.

In order to scale the HEMP thruster down it is from this point of view advantageous using a small discharge chamber.

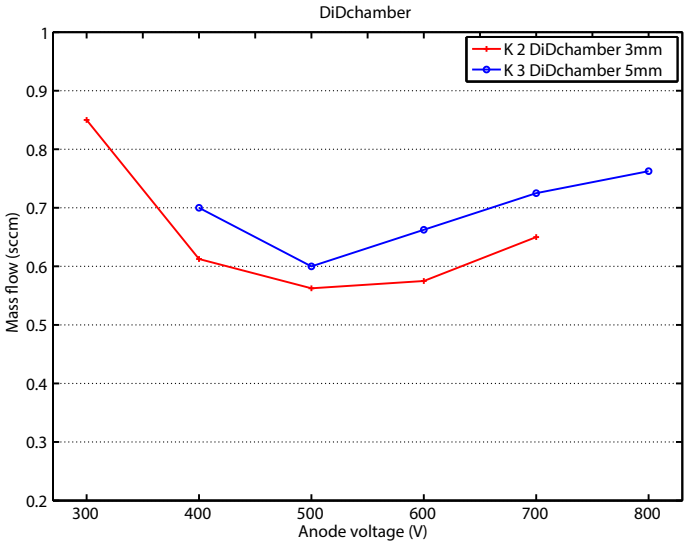

Figure 6. Minimal mass flows versus anode voltage for different inner diameters of magnets.

2. Divergence efficiency

In Fig. 7 the Faraday currents for different outer magnet diameters are shown which corresponds to strength of magnetic field. All curves show the typical hollow cones shape with a maximum emission around $\pm 60°$. In order to compare the different measurements which are recorded on different anode currents the peaks of the curves are normalised.

The divergence efficiencies for 10 and 20 mm are equal and then decreasing for increasing diameters. This can be seen by the moving of maximum to higher angles with increasing diameter and the parallelity

of sides. Only the 10 and 20 mm curves are crossing each others on high angles which explains the equality of divergence efficiencies.

Nevertheless, the curves are similar in shape and the values of divergence efficiency have only a small variation. In this test series in combination with that voltage the variation is relatively large from 0.5 to 0.37. In DiDchamber is the variation of efficiencies within the same operation point below 0.05, in DoMagnet for the other voltages below 0.10, in DistMagnet around 0.01, NumberMagnet below 0.04, and for combined DiMagnet-DiDchamber $0.10 - 0.17$.

So impact of the examined geometry parameters is limited and exclusively important in case of optimisation of an existing device. For a fundamental modification which is needed in our case the impact is too low.

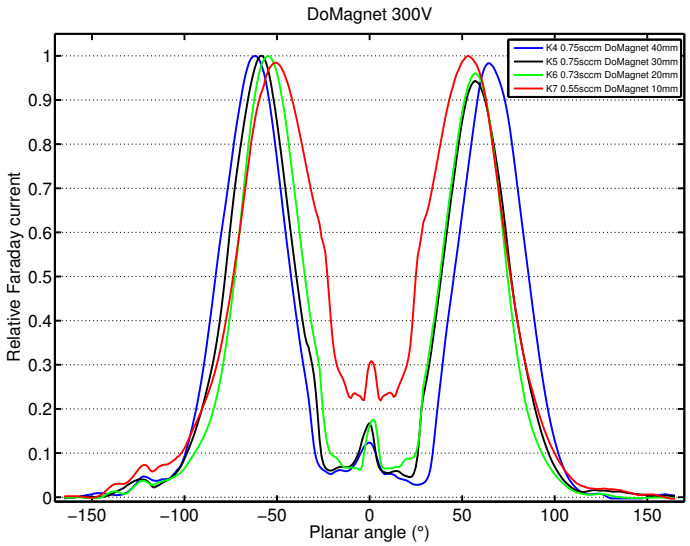

Figure 7. Faraday currents (relative to it's respective maximum) versus planar angle for different thruster configurations of the same test series.

3. Acceleration efficiency

In Fig. 8 the acceleration efficiencies for different outer magnet diameters are shown. The markers are RPA measurements which can only be performed where beam current is high enough for a reasonable signal-to-noise-ratio. In order to obtain a total acceleration efficiency the measured values needs to be extra- and interpolated which is done by a fit (see section A, visualised with the dashed line).

The maximum of acceleration efficiency is at maximum of beam current around $\pm 60°$ while for larger angles the efficiency decreases. The curve of 20 mm configuration is maximum in total acceleration efficiency with 0.865 while the other two efficiencies are about 0.02 smaller. Although the efficiencies away from beam current peak at $\pm 60°$ are much lower for 20 mm curve, the angular dependant efficiencies are weighted with the beam current so that the dip could be counteracted.

For the others test series the acceleration efficiencies varies for the same operation point in DoMagnet (other operation points) around 0.01, DistMagnet below 0.04, NumberMagnet below 0.04, combined DiMagnet-DiDchamber below 0.035.

Again the efficiencies vary exclusively on a small range which makes this parameter insignificant for downscaling considerations.

4. Discussion

Although the impact on downscaling is limited, the optimum values of the probed geometries are given in Table 2. For operation space (OS) the configurations with minimal mass flow (second column) and minimal anode current (third column) are noted. A low current corresponds to a low thrust via the ion current. In the last two columns the configurations with the maximum divergence and acceleration efficiencies are

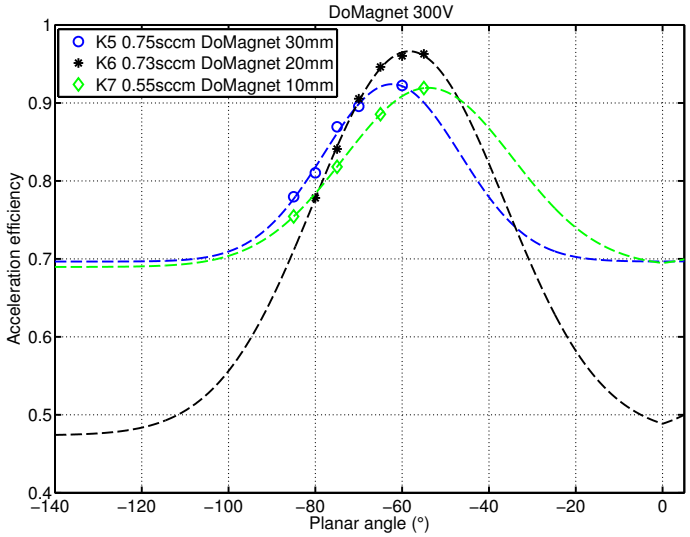

Figure 8. Acceleration efficiencies (markers) with corresponding fit (dashed lines) for different thruster configurations of the same test series at 300 V anode voltage.

shown, respectively. It must be mentioned that the real optimum parameters may be in between the probed values.

The optimum values are similar in each column so that it seems possible to build a prototype which has improved characteristics in all categories. Nevertheless must be considered that these changes is only fine tuning of thruster operation due to its low impact and is not appropriate to build a completely new thruster.

Parameter	OS mass flow	OS anode current	Divergence	Acceleration
DiDchamber	3 mm	5 mA	undetermined	5 mm
DoMagnet	20 mm	20 mm	10/20 mm	20 mm
DistMagnet	5 mm	5/10 mm	5 mm	5 mm
NumberMagnet	> 2	> 2	3	2

Table 2. Optimum values for the studied configurations

C. Anode Material

In Figs. 9 and 10 the derivative of RPA current calculated as difference of measurement values (coloured marker) and as derivative of fit is plotted. For several angles data of baseline thruster K5 with aluminium anode and K26 with brass anode in the two Figs., respectively, is shown at 500 V and 0.7 sccm.

The current decrease at the highest retarding voltage is shown which lies with the aluminium anode $50 - 45$ V and with the brass anode about 5 V below anode voltage. These values are associated with an uncertainty of below 5 V due to the large voltage step of retardation voltage. This uncertainty, however, is low compared to the difference. The same values are observed for other operation points and other thruster configurations.

It can be stated that the anode material has an influence in the maximum acceleration voltage of ions. The aluminium anode causes a voltage difference of about 40 V compared to brass voltage which effects acceleration efficiency. For the three studied operation points an acceleration efficiency increase of 0.022 to 0.04 can be reported.

The exact reason of the material dependance is unclear. Possible causes are different work functions, oxide layers or ionisation energies of free metal atoms. Further tests with other anode materials may be necessary.

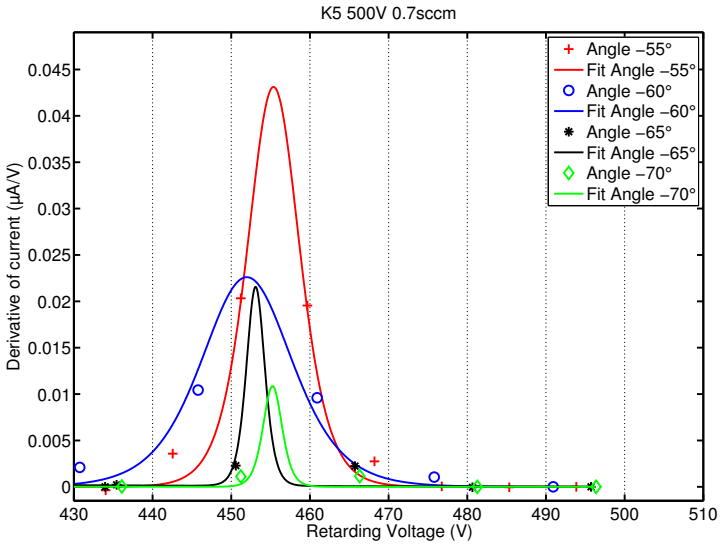

Figure 9. Derivative of RPA current is plotted as difference of measurement values (coloured markers) and as derivative of fit (solid line). For several angles data of baseline thruster K5 with aluminium anode is shown at $500\,\mathrm{V}$ and $0.7\,\mathrm{sccm}$.

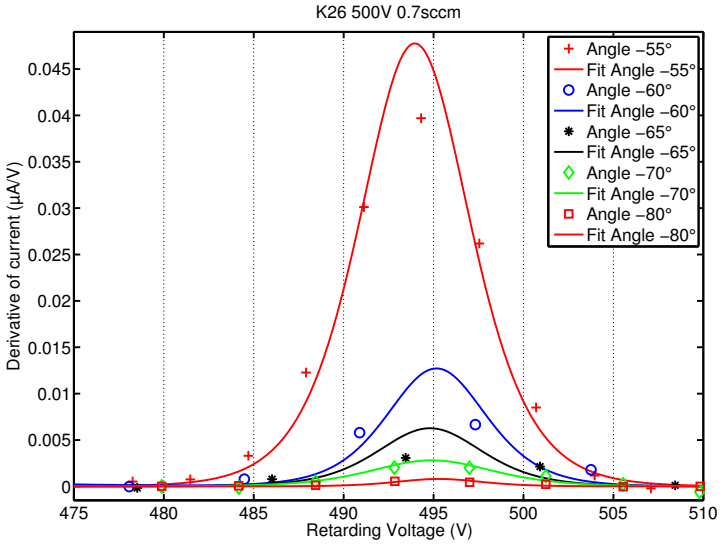

Figure 10. Derivative of RPA current is plotted as difference of measurement values (coloured markers) and as derivative of fit (solid line). For several angles data of configuration K26 with brass anode is shown at $500\,\mathrm{V}$ and $0.7\,\mathrm{sccm}$. It differs from baseline thruster K5 exclusively in anode material.

IV. Conclusion

The miniaturization of a HEMP thruster is experimentally studied and a functioning µHEMP was designed and characterized. The minimum achieved thrust was 50 µN and 70 s by 350 V.

By changing the geometry of thruster the impact to operation space and divergence as well as acceleration efficiency was studied. A small influence was measured and it seems possible to build a prototype which is optimised in all tested categories. Nevertheless, the impact is limited and there is no evidence that a complete new thrust range can be reached with these measures.

Surprisingly the anode material has an influence in acceleration efficiency. It was shown that the brass anode demonstrates an up to 4% higher efficiency than aluminum anode. Nevertheless the reasons are not yet understood. Further tests with different anode materials needs to be performed.

The characterisation shows the complexity of the thruster physics and the necessity of a more detailed ion velocity diagnostics.

References

[1]Tim Brandt, Rodion Groll, Frank Jansen, Ulrich Johann, Andreas Keller, Holger Kersten, and Claus Braxmaier. Magnetohydrodynamics and particle-in-cell codes simulation of plasma processes in micro hemp-thrusters. Number IEPC-2013-145 in 33rd International Electric Propulsion Conference, Washington, USA, 2013.

[2]A Genovese, A Lazurenko, N Koch, S Weis, M Schirra, B van Reijen, J Haderspeck, and P Holtmann. Endurance testing of hempt-based ion propulsion modules for smallgeo. Number IEPC-2011-141 in 32nd International Electric Propulsion Conference, Wiesbaden, Germany, 2011.

[3]A Keller, P Köhler, W Gärtner, B Lotz, D Feili, P Dold, M Berger, C Braxmaier, D Weise, and U Johann. Feasibility of a down-scaled hemp-thruster. Number IEPC-2011-138 in 32nd International Electric Propulsion Conference, Wiesbaden, Germany, 2011.

[4]G. Kornfeld, N. Koch, and G. Coustou. The highly efficient multistage plasma (hemp) thruster, a new electric propulsion concept derived from tube technology. 4th IEEE International Conference on Vacuum Electronics, 2003.